Evaluating the Possible Impacts Climate Change May Induce on Fermilab's Radioactive Air Emissions

Anne Murray[a] Matthew Quinn[b] Diane Reitzner[c]

[a]*Purdue University, 2021 SIST Intern*
[b]*Fermilab, Associate Section Head and Senior Radiation Safety Officer*
[c]*Fermilab, Environment, Safety, & Health Section and Radiation Physicist*

Abstract. Climate change is an inevitable consequence of human activity, and humans must focus on minimizing it and adapting to its anticipated effects. Fermi National Accelerator Laboratory, otherwise known as "Fermilab", is no exception to this principle, and the facility must ensure public safety while its operations distribute airborne radionuclide emissions. Climate change is anticipated to modify atmospheric conditions, including wind patterns, and these effects may alter how Fermilab's radioactive emissions are administered to the surrounding area. This study will use the University of Illinois (U of I) climate model to predict future local climatic and weather conditions around Fermilab's campus. These projections, along with Fermilab's radioactive emissions, will act as inputs for CAP-88, a U.S. Environmental Protection Agency (EPA)-based computer model, to predict the surrounding population's doses and exposure to any airborne radioactivity emitted from Fermilab. If the resulting radionuclide doses challenge the federal exposure limit, then Fermilab may have to alter its operations and project designs to reduce these emissions.

1. Introduction

Previously, climate change was a natural process resulting from external changes such as solar radiation, volcanic eruptions, greenhouse gases (GHGs), and changes in the Earth's orbit. Before humans, GHGs, like carbon dioxide, were the natural result of microbial, plant, and animal respiration, as well as volcanic activity, and they all contributed to the greenhouse effect (Denchak, 2021). This effect is a natural process that warms the Earth through the absorption and reflection of the sun's infrared energy by GHGs in the atmosphere. GHGs absorb and re-radiate the sun's energy in all directions, including back towards the Earth's surface, consequently warming the planet (NASA, 2021). Before humans, the levels of GHGs in the atmosphere remained relatively stable due to Earth's slow, natural processes. However, human activities, like the combustion of fossil fuels, agricultural land use, and other industrial activities including manufacturing, have amplified the GHGs in the atmosphere, including, but not limited to, carbon dioxide, methane, and nitrous oxide. These gases increase the rate at which the greenhouse effect occurs, consequently increasing global temperatures at a rate remarkably faster than natural causes have. Since 1880, the average global temperature has increased by about 1° C, and ⅔ of this warming has occurred since 1975 as the rate of GHG-producing human activities has very quickly grown (Earth Observatory, 2020). While the natural causes emitting GHGs still occur today, their influence is too minimal to explain the rapid rate of warming the planet has experienced in recent decades.

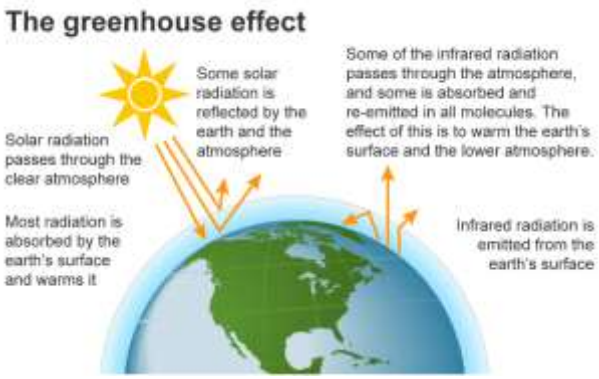

Figure 1. A visual representation of the greenhouse effect (EIA, 2021)

The characteristics and magnitude of climate change depend on several factors, like GHG composition and concentration, as well as the geography of any region. Besides the increase in temperature, climate change may cause more frequent and intense weather events, like droughts, storms, and heatwaves, as well as rising sea levels. With these changes, atmospheric conditions are altered and may affect the distribution of airborne particles, including the radioactive isotopes Fermilab emits while running its accelerators and beamlines. Different atmospheric patterns may increase the surrounding population's exposure to Fermilab's emitted isotopes, and since Fermilab ensures these airborne doses remain below the regulated limit of 10 millirem (mrem) by the EPA, the lab's future operations may be compromised to remain under the threshold exposure (EPA, 2000). Even if Fermilab's current emissions remain below the regulated dosage, the lab has plans to increase power and add new projects that may increase its radioactive emissions, so understanding how these emissions may vary coupled with climate change is vital for Fermilab's future.

2. Procedure

2.1 The University of Illinois Climate Model

Climate models are computer simulations that summarize Earth's climate systems. They use previous climate and weather records combined with projections to calculate future atmospheric conditions, temperatures, pressures, wind patterns, and humidities, enabling projections of short-and-long-term climate patterns and weather events. The climate model used in this study was developed by the University of Illinois and predicts these variables in the Fermilab region for the middle and end of this century (Zobel, 2017). This report will highlight some of the uniquely advantageous aspects U of I's model offers that are relevant to its selection for this project.

One unique ability U of I's model offers is dynamical downscaling. This feature utilizes high-resolution geography and topography simulations to extrapolate the effects that large-scale climate processes have on smaller, localized scales. Downscaling is necessary for accurate projections as it considers the localized area's topography, better capturing its spatial and temporal variations that contribute to localized weather patterns. Ultimately, this leads to more accurate predictions regarding the frequency, intensity, and type of extreme weather events in a

specified local area. With U of I's 12x12 kilometer (km) resolution, these projections are specific to the Fermilab area and will more precisely predict the region's future weather events (Zobel et. al, 2018).

A second highlight is the model's systematic ability to overcome skewed biases. Biases in climate models occur from limited data input or projection calculations that do not represent all possible climate perspectives. While there are a variety of pre-existing global-scale climate models, each comes with its own limitations, including over-or-under-estimating weather events, precipitation, or the effects of GHGs on rising temperatures. U of I addresses these implicit biases by combining three different climate models with varying estimations regarding how the mean global temperature will rise with a doubling of CO_2: the Geophysical Fluid Dynamics Laboratory Earth System Model 2 from National Oceanic and Atmospheric Administration which anticipates the lowest rise at 2.38^o C, the Community Climate System Model 4 from the National Center for Atmospheric Research which estimates an average temperature increase of 2.9^o C, and the Hadley Centre Global Environment Model Version 2 from the Met Office Hadley Center which projects the highest temperature rise at 4.5^o C (Zobel et al., 2017). Including this range of predictions allows U of I's model to incorporate high, low, and average weather and climate projections, thus minimizing the typical bias a singular climate model may experience.

Model	Geophysical Fluid Dynamics Laboratory Earth System Model 2	Community Climate System Model 4	Hadley Centre Global Environment Model Version 2
Developer	NOAA/Geophysical Fluid Dynamics Laboratory	National Center for Atmospheric Research	Met Office Hadley Center, UK
Mean global temperature increase with a doubling of CO2	2.38 C	2.9 C	4.5 C

Figure 2: A table describing the three global climate models used within U of I's model and their temporal sensitivity to a doubling of CO_2

2.1.1 Climate Scenarios Evaluated

The specific climate scenarios applied towards this study use two scenarios highlighted by the Intergovernmental Panel on Climate Change (IPCC), RCP4.5 and RCP8.5. These different scenarios are named "Representative Concentration Pathways" (RCPs), followed by a quantitative value to characterize their climate scenario. RCPs predict how GHG concentrations in Earth's atmosphere can change as a direct result of human activity. The numbers indicate the radiative forcing level through a land-use-land cover measured in watts/m^2 (Met Office, 2018). The IPCC developed four pathways ranging from RCP2.6 - RCP8.5 where a larger RCP value indicates more GHG emissions occur, resulting in higher atmospheric GHG concentrations.

If human GHG emissions are not regulated and instead increase with a rise in population and energy demand, a "business as usual" scenario, represented by RCP8.5, predicts an end-of-century temporal increase of 3.7^o C (IPCC, 2014). This worst-case scenario anticipates a world that continues to generate energy through coal-fired power with a transportation system dominated by gasoline-fueled individual vehicles. While this scenario is considered unlikely due

to the push for increased regulation and the introduction of new renewable technologies, it was used for this study so Fermilab could analyze how their operations could be affected in an extreme scenario.

The second RCP used in this study takes an intermediate approach, RCP4.5, which estimates GHG emissions will become more heavily regulated, resulting in an end-of-century temporal increase of only 1.8^{o} C (IPCC, 2014). This includes a renewable-based energy generation system with a mix of private and public transportation where some vehicles are run by electricity. While there is an even lower RCP, it seems too optimistic to be realistic - it anticipates a high effort to curb GHG emissions by solely using renewable energy sources, implementing large-scale GHG emission capturing programs, and having an increased use of public transportation where all remaining individual vehicles are fueled electrically. Unfortunately, this does not seem to be realistically achievable on a large scale, so this scenario was not used for this study. However, excluding this scenario still enables this study to encompass the more conservative projections of climate change as represented through RCP4.5.

For U of I's model, RCP4.5 and RCP8.5 were each evaluated at two decadal times - "Mid" indicates the middle of the century, representing years 2045-2054, and "End" indicates the end of the century, representing years 2085-2094. The 4 scenarios modeled for this project are abbreviated as follows: RCP4.5 Mid, RCP4.5 End, RCP8.5 Mid, and RCP8.5 End.

2.2 CAP-88

The second computer program used in this study is CAP-88, a US EPA computer model used as a compliance tool under the National Emissions Standard for Hazardous Air Pollutants (EPA, 2021). Its purpose is to estimate the public's dose and risk from airborne radionuclide emissions. For this study, CAP-88 utilizes momentum-based Gaussian plume modeling to estimate the average airborne dispersions of Fermilab's radioactive particles and evaluates the low-level chronic exposure the public may experience under varied climatic and weather conditions, the outputs from the U of I climate model.

Modeling the airborne radionuclide emissions, or plumes, the public receives from Fermilab's campus is assessed through ten radial distances, each spanning sixteen directions. The radial groups cover distances 1.6 km through 80 km from Fermilab, extending through Northern Illinois and its borders with Wisconsin and Indiana. Before any atmospheric conditions, like wind patterns, are put into CAP-88, the program assumes a uniform distribution of particles within all radii. When U of I's data is added to this program, the radionuclide distributions are calculated in tandem with the projected atmospheric conditions, disrupting the initial uniform distribution.

While Gaussian plume modeling is built into CAP-88, a brief explanation on how the process works will be described. This kind of dispersion modeling assumes the maximum concentration at any distance downwind from the source (x) appears at the plume's centerline, and this centerline concentration decreases as distance from the source increases. This implies that, at any x, the concentration of radionuclides decreases exponentially as their distance from the centerline increases. The sources of these emissions, while dispersed throughout an area on Fermilab's campus, are assumed to share one location at the same height, H, and each stack's

contributions to airborne radionuclides are additive. As the emissions leave their source, they do not immediately disperse horizontally, as the momentum of the emissions carries the radionuclides some height, He, along the z-direction, creating ΔH, a plume rise (Cossairt & Quinn, 2021). The emissions are evaluated along the plume path summarized in *Figure 3*.

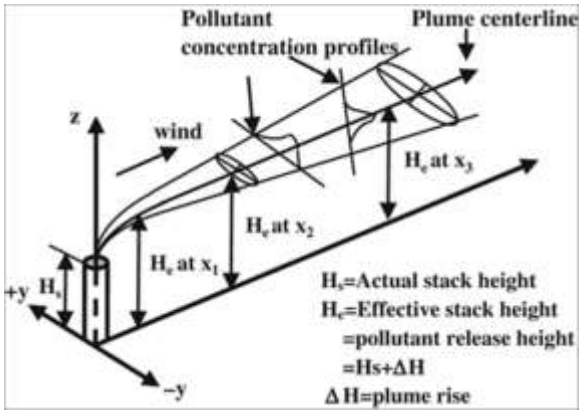

Figure 3: A visual summary of momentum-based Gaussian plume modeling

2.2.A CAP-88 Version 3

There were two CAP-88 programs utilized to complete this project, CAP-88 Version 3 (V3) and CAP-88 Version 4 (V4). V3 was used to calculate the future distribution patterns of wind based on the inputs of wind speed and direction from U of I's climate model. Using lateral wind directions, sigma-h, V3 analyzed the horizontal standard deviation of the projected wind data to calculate the atmospheric stability class of the wind by daily increments. Atmospheric stability measures the atmosphere's tendency to deter wind parcels' vertical motion; a stable atmosphere is achieved when a wind parcel shares the same temperature with its surrounding air, resisting vertical movement, while instability occurs when the wind parcel is warmer than its surroundings, causing the parcel to rise and create storms (Cossairt & Quinn, 2021). These stability classes, shown in *Figure 4*, are categorized into qualitative classes to characterize atmospheric conditions.

Surface Wind Speed (at 10 m) knots	Day Incoming solar radiation Strong	Moderate	Slight	Night Thinly overcast or >4/8 Low cloud	<3/8 Cloud
< 3.9	A	A – B	B		
2.9 – 5.8	A – B	B	C	E	F
5.8 – 9.7	B	B – C	C	D	E
9.7 – 11.7	C	C – D	D	D	D
> 11.7	C	D	D	D	D

* A – Extremely unstable, B – moderately unstable, C – slightly unstable, D – neutral, E – slightly stable, F – moderately stable (WHO, 1989).

Figure 4: The characteristics of each atmospheric stability class

V3 outputs stability classes based on the wind data's horizontal standard deviations, and these outputs then acts as an input for V4's meteorological data. The technological capabilities of U of I's climate model were confined to daily horizontal standard deviation averages for the future decades and were not able to provide hourly estimates. As a result, every day for both the temporal scenarios and their mid-and-end century decades was qualified as stability class D, the neutral class, possibly excluding any short-term outlier classes that may have occurred throughout the day. The generated stability classes were assigned to their respective directions based on a sixteen-point compass, matching V4's sixteen-directional output. After calculating and sorting the atmospheric stability classes into their respective directions from V3, another computer program, STARGET, is used to convert the file format from V3 into a version that is compatible as an input for V4.

2.2A.1 Population Estimations

A secondary dataset file required as an input for V4 summarizes the distribution of the surrounding population within the ten radial distances evaluated. For this study, the ten radii, in kilometers, are as follows: 1.6, 3.2, 4.8, 6.4, 8.0, 16.1, 32.2, 48.3, 64.4, and 80. Each radial distance was divided into sixteen directions - north, north-northwest, northwest, west-northwest, west, west-southwest, southwest, south-southwest, south, south-southeast, southeast, east-southeast, east, east-northeast, northeast, and north-northeast - the same used for describing atmospheric stability in the V3 wind file. For each radius, the number of people residing within its limit was estimated using 2019 US Census Bureau projections. The estimated population as provided by the Bureau was per township, and each township was assumed to have an equal population distribution within its limits.

Figure 5: The largest radial area analyzed surrounding Fermilab (80 km)

Each radius was overlaid with a sixteen-point compass to estimate which counties were to be considered for each directional sector, as shown in *Figure 6*. Then, each county was divided into its townships, overlaid by the same compass centered at Fermilab's location, and the population estimates were recorded corresponding to their proportional directional area. Refer to *Figure 7 for* an example of how one township within DuPage County was assigned. This process was repeated for each township within every county for all ten radii.

Figure 6: A photo showing the process of overlaying the 80 km radius, centered at Fermilab's campus, the sixteen-point compass, and the Illinois county map.

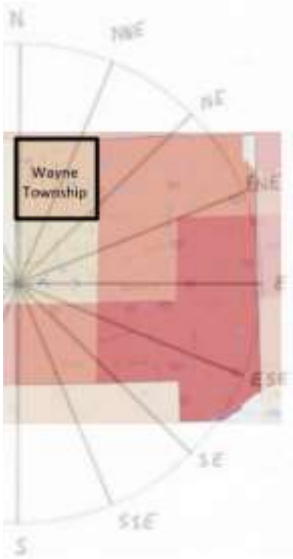

Figure 7: An example on how the populations were assigned within DuPage County. The boxed township's (Wayne's) total population was divided with the following proportions: 30% north, 50% north-northeast, and 20% northeast.

2.2B CAP-88 Version 4

With the wind and population data files completed, accessing the remaining data inputs for V4 was straightforward. Recall 2 RCPs were evaluated at 2 decadal timeframes and, for each scenario, the meteorological data, including annual precipitation, annual ambient temperature, and absolute humidity, were averaged by the decade. Illinois's agricultural data, including livestock and vegetation densities, were calculated within V4 automatically. The agricultural data is necessary due to biomagnification, a process that estimates the uptake of toxins, like Fermilab's emitted radionuclides, through the food chain. Biomagnification describes how the concentration of radionuclide doses ingested by humans, the top of the food chain, are the additive result of their food sources' doses from lower trophic levels (Gupta, 2020). For example, if grasses are exposed to radionuclides and are then eaten by livestock, the livestock receive the ingested grass's radiation dose. When these livestock are then consumed by humans, humans are exposed to all the radiation concentrated in the lower trophic levels, the grass and livestock combined. This means humans are at risk from both airborne inhalation radiation and surface-deposited biomagnification radiation, so V4 includes both these pathways in its analysis. Finally, all the nuclides Fermilab emits, including their chemical form (water vapor or pure particulate), type (the particulate's speed or the inhalant's physical state), size, and release rate, were provided by Fermilab staff based on emission reports and are listed in *Figure 8*.

Chn	Nuclide	Chem Form	Type	Size	RR1	RR2	RR3	RR4	RR5
0	N-13			0.00...	2.417e-01	3.295e+00	8.170e-01	1.490e+00	7.864e-01
0	C-11	Particulate	M	1.00...	5.287e-01	3.946e+00	8.588e-01	2.101e+00	5.405e+00
0	Ar-41			0.00...	1.809e-02	9.383e+00	7.322e-01	6.282e-02	2.188e+00
0	O-15			0.00...	3.371e-02	7.223e+00	8.032e-01	2.238e-01	1.661e-03
0	Br-77	Particulate	M	1.00...	0.000e+00	0.000e+00	5.999e-05	0.000e+00	0.000e+00
0	Br-82	Particulate	M	1.00...	0.000e+00	0.000e+00	1.454e-04	0.000e+00	0.000e+00
0	Ru-97	Particulate	M	1.00...	0.000e+00	0.000e+00	5.911e-06	0.000e+00	0.000e+00
0	H-3	Tritiated Wat...	V	0.00...	1.628e-02	1.983e-02	1.965e+00	4.845e-01	3.948e+00

Figure 8. Fermilab's emission characteristics; the columns read "Chn" for chain length, "Type" for the type of nuclide form where "M" indicates a particulate with a medium dispersal speed and "V" indicates a vapor-based inhalant, and "RRN" for released radionuclide count

3. Results

3.1 Maximally Exposed Individual

The most important statistic is the maximally exposed individual (MEI), the person who receives the most concentrated dose of Fermilab's radioactive emissions. RCP4.5 End has the lowest MEI at 8.96E-3 mrem, or .0869% of the federal limit, while RCP8.5 Mid has the highest MEI at 1.00E-2 mrem, about .10% of the federal limit. Both RCP8.5 scenarios have higher MEIs than the RCP4.5 scenarios, and the end-century scenarios have a more significant difference between their MEI values than the mid-century scenarios since the later decade is exposed to the altered climate conditions longer. For the mid-century scenarios, the RCP4.5 Mid MEI is 1.6E-4 mrem smaller than the RCP8.5 Mid MEI, and for the end-century scenarios, the RCP4.5 End

MEI is 1.6E-3 mrem smaller than the RCP8.5 End MEI. This means the end-century scenarios have a ten times larger difference in MEI than the mid-century time frame. For each scenario, the MEI shares the same location at 800 meters (m) northwest of Fermilab's campus, which lies within the lab's adjacent neighborhood.

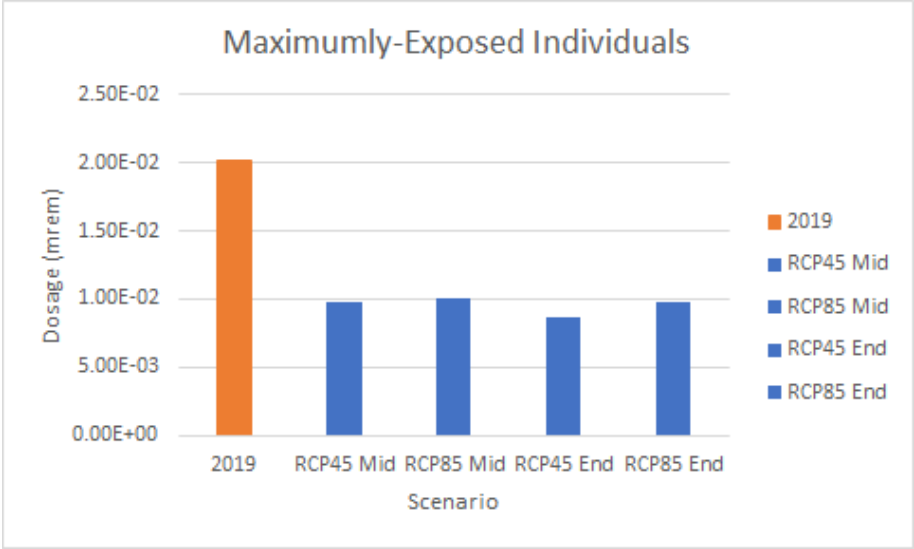

Figure 9: MEI results across all 4 analyzed scenarios compared to the MEI from 2019

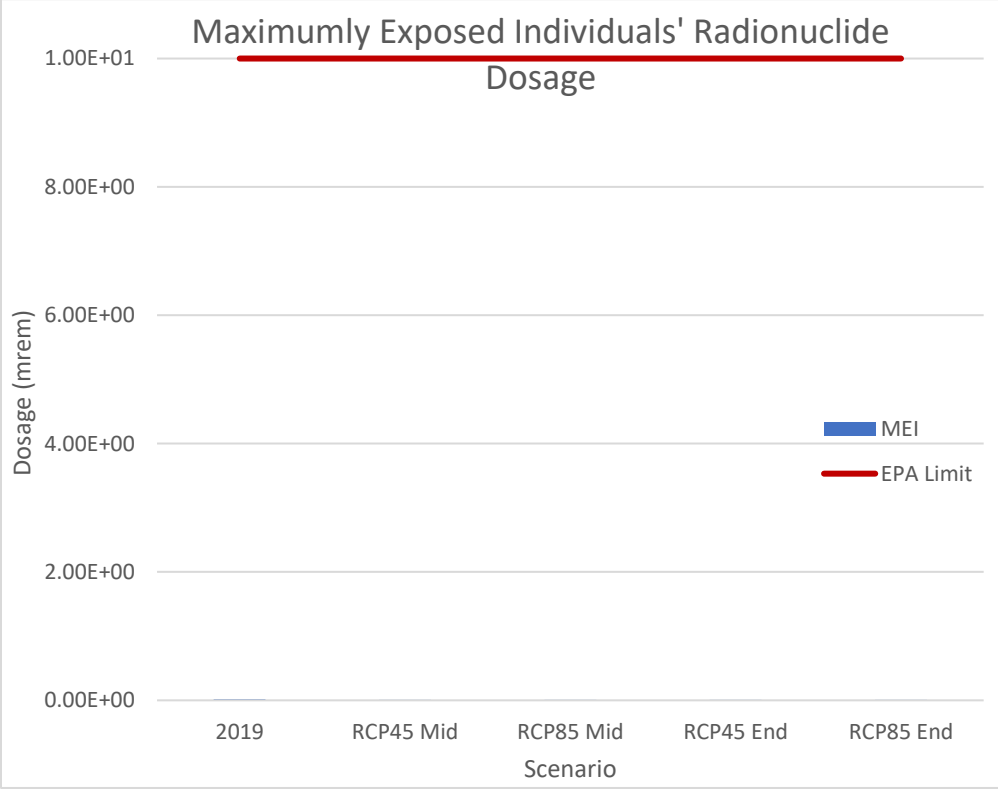

Figure 10: The MEI values from *Figure 9* scaled against the EPA limit

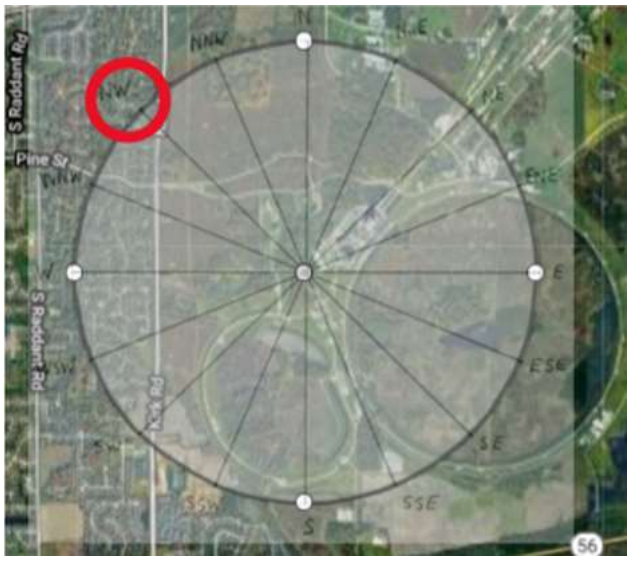

Figure 11: The location of the MEI across all 4 scenarios

3.2 Collective Dosages

A second significant statistic comes from understanding the relationship between the distance from Fermilab's campus and the dose of radiation received. As distance from campus increases, the individual and collective population doses decrease, as shown in *Figure 12*. This figure compares the collective population dose Naperville receives, which is only about 12,050 m from Fermilab, with the collective dose Harvard experiences, which is about 72,200 m from Fermilab. On average, Harvard only receives 2.74% of Naperville's dosage and is located nearly 600% further away from Fermilab than Naperville. *Figure 13* scales the Collective Population with the EPA limit to show how far below these dosages are from the threshold. Despite representing a collective dosage, these values are still significantly smaller than the MEI due to their distance from campus.

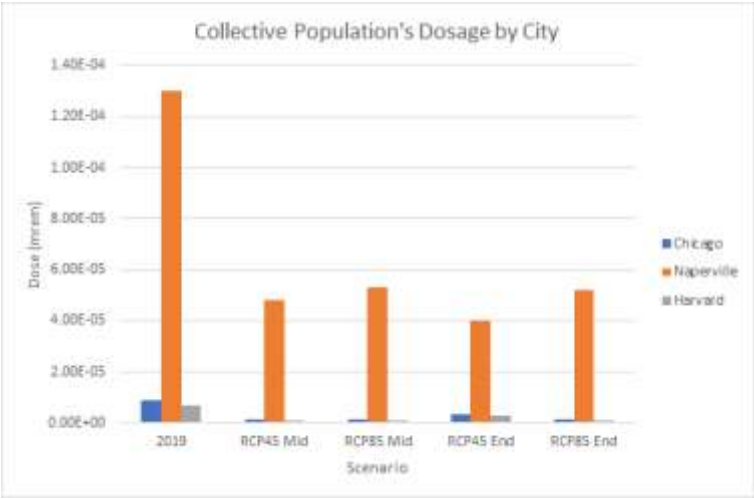

Figure 12: The collective radionuclide dosages of the entire population that these cities receive compared against the collective dosages from 2019

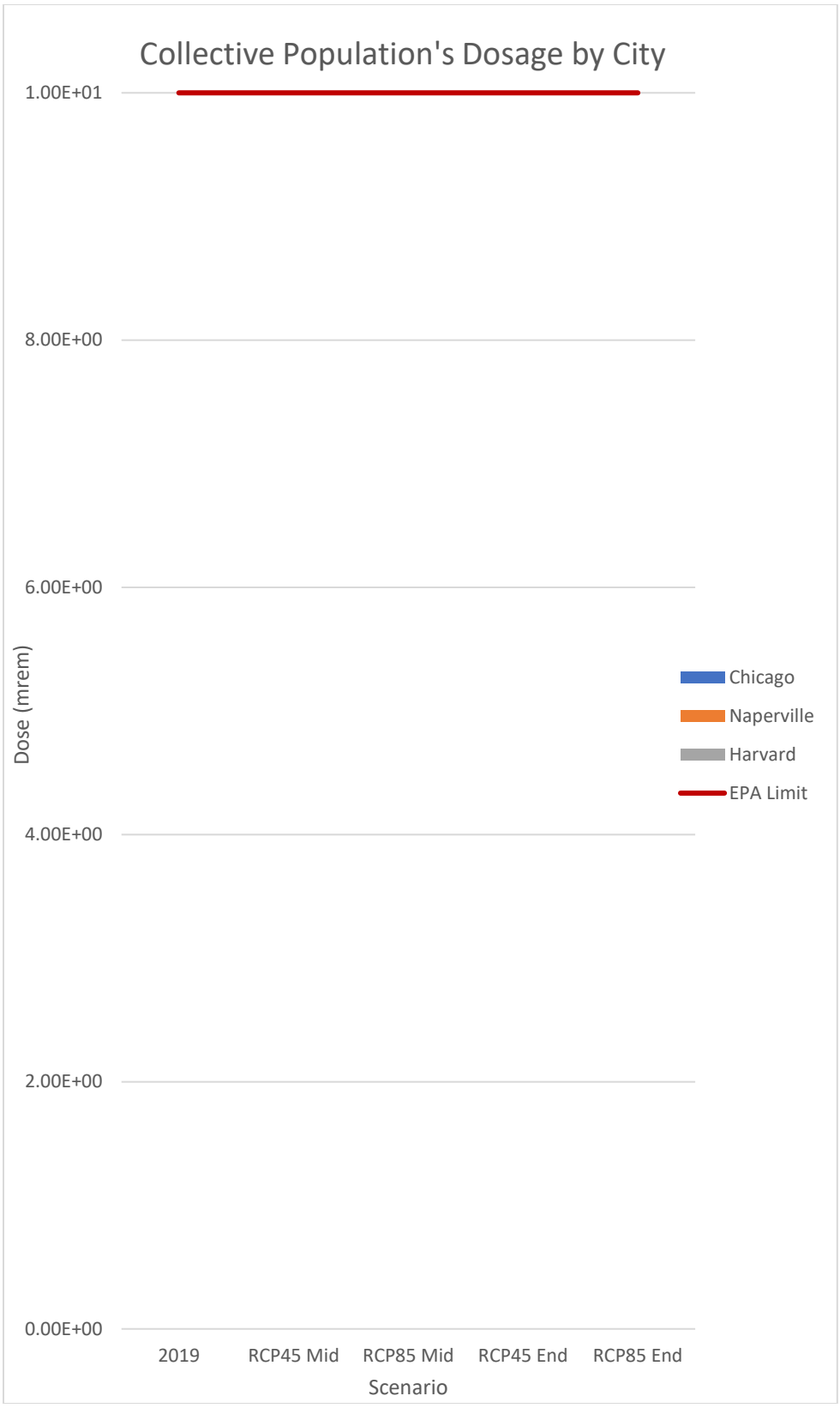

Figure 13: The collective doses from *Figure 12* scaled against the EPA limit

3.3 Historic Comparisons

For both MEI and collective dosage, 2019's emissions were included as a base value to compare the future climate scenarios against, and those doses are all larger than any RCP scenario. One theory for this trend is that climate change will alter atmospheric conditions to become less stable, consequently increasing wind speed and power. This change, while decreasing MEI and the doses surrounding Fermilab, will increase the range of the doses distributed. CAP-88 limits its analysis at 80,000 m and, for every distance and direction evaluated, 2019 has higher doses than any RCP scenario. However, if distances greater than 80 km were evaluated, it is expected that 2019's doses would cover a remarkably smaller total area than either RCP scenario since its doses are more concentrated.

3.4 Results by Radionuclide

For every scenario across both the MEI and collective dosages, Argon-41 is the radionuclide with the largest dose, averaging at 4.8E-3 mrem for MEI and 1.3E-1 mrem for collective doses. Tritium, H-3, is the second most concentrated radionuclide emission, and Tc-97 is the least concentrated dosage averaging 7.7E-16 mrem for the highest individual dosage. As indicated by the MEI's shared location 800 m NW from campus, the direction with the most concentrated direction overall is northwest, indicating southeast is the dominant wind direction near Fermilab.

Nuclide Effective Dose Equivalent Summary										
Nuclide	RCP45 Mid		RCP85 Mid		RCP45 End		RCP85 End		Total by Nuclide	
	Individual	Collective	Individual	Collective	Individual	Collective	Individual	Collective	Individual	Collective
N-13	1.29E-03	2.91E-03	1.29E-03	2.95E-03	1.13E-03	2.53E-03	1.26E-03	2.85E-03	4.97E-03	1.12E-02
C-11	3.27E-03	1.86E-02	3.31E-03	1.86E-02	2.87E-03	1.66E-02	3.18E-03	1.81E-02	1.26E-02	7.19E-02
Ar-41	4.83E-03	1.37E-01	4.97E-03	1.36E-01	4.29E-03	1.30E-01	4.70E-03	1.34E-01	1.88E-02	5.37E-01
O-15	2.96E-04	7.91E-05	2.65E-04	8.16E-05	2.39E-04	6.43E-05	2.88E-04	8.67E-05	1.09E-03	3.12E-04
Br-77	4.78E-08	5.31E-06	4.95E-08	5.43E-06	4.13E-08	4.71E-06	4.71E-08	5.40E-06	1.86E-07	2.09E-05
Br-82	6.61E-07	6.77E-05	6.85E-07	6.91E-05	5.73E-07	6.04E-05	6.51E-07	6.87E-05	2.57E-06	2.66E-04
Ru-97	4.21E-09	4.67E-07	4.37E-09	4.78E-07	3.65E-09	4.14E-07	4.15E-09	4.75E-07	1.64E-08	1.83E-06
Tc-97m	2.81E-14	4.50E-12	2.92E-14	4.62E-12	2.41E-14	3.93E-12	2.78E-14	4.59E-12	1.09E-13	1.76E-11
Tc-97	8.00E-16	1.06E-13	8.31E-16	1.08E-13	6.87E-16	9.24E-14	7.91E-16	1.08E-13	3.11E-15	4.14E-13
H-3	1.51E-04	1.58E-02	1.56E-04	1.57E-02	1.65E-04	6.76E-02	1.47E-04	1.57E-02	6.19E-04	1.15E-01

Figure 14. A table summarizing the dose equivalents by nuclide for each evaluated scenario

4. Limitations

The limitations regarding the validity of these results must be understood to disclose the context this study covers. Firstly, predicting climate and weather patterns nearly 80 years from now has substantial room for error. Even predicting weather 10 days in the future has an average error of 50% (NOAA, 2021). While climate is significantly easier to predict than the weather, both factor into the meteorological data used as inputs for CAP-88. U of I's climate model is an impressive technological feat, but it is prone to some margin of error that can only be confirmed once the end of the century occurs when the weather and climate are experienced first-handedly.

A second pressing limitation comes from the uncertainty in predicting how human actions will change atmospheric GHG concentrations over the century, as the temporal increase

will be proportional to these emissions. GHG emissions may increase with a growing population that demands more energy generation, or they may decrease with improved power efficiency and emission regulations. While 2 RCPs were used to reflect these possibilities, the actual RCP may lie somewhere over, under, or in-between the RCPs used for this study. This limitation is not only dependent upon the population size relying on energy production, but also how this energy is generated, as renewable sources will not contribute to GHG emissions. However, another source of error comes from the numerical value of the future population itself. The 2020 US Census Bureau has not yet been released as of July 2021, so this study used the 2010 Census's projection for 2019 population values. CAP-88 takes this population input and projects it for future decades, and CAP-88's calculation may also be prone to some error. As a result, the actual population, as well as any GHG and temporal values at the end of the century, may be higher, lower, or somewhere in-between the estimated values used in CAP-88.

An additional cause for possible error comes from within the CAP-88 and U of I climate model programs; they required simplifying the climate model's data through averages and were only capable of devising two decadal-length temperature scenarios. While the climate model generates wind speed and direction in 3-hour increments, CAP-88 only accepts daily averaged wind values, skewing the input data by any outliers that may have over-or-undervalued the actual values generated. Similarly, climatic data, like annual precipitation and annual ambient temperature, were averaged by decade as this study only assessed two decadal-length timeframes and not the twenty individual years for each of the RCP scenarios. Finally, U of I's climate model has some missing analog data, leaving certain periods out of the analysis, once again causing oversimplified averages to be used as inputs for CAP-88. While analyzing these uncertainties is beyond the available time frame for this project, these limitations may form the basis for future studies.

5. Conclusion

Each of the 4 scenarios shares the same conclusion - with Fermilab's current operations, radioactive air emissions will remain well below the EPA threshold. This means Fermilab operations will not be impacted by climate change in the long term and that the lab has ample opportunities to increase power to support future projects safely. Despite the limitations described above, the initial conclusion remains valid, denoting operations may continue and even increase power. This claim remains since any sources of error, no matter which magnitude they may occur in, should not have enough influence to consequently alter the resulting conclusion. Even as Fermilab installs new operations and increases its power, its emissions will remain well below the EPA limit, ensuring public safety.

6. Acknowledgements

This manuscript has been authored by Fermi Research Alliance, LLC under Contract No. DE-AC02-07CH11359 with the U.S. Department of Energy, Office of Science, Office of High Energy Physics.

References

Cossairt, J. D., & Quinn, M. (2021). Induced Radioactivity in Environmental Media. In *Accelerator radiation physics for personnel and environmental protection*. essay, CRC PRESS.

Denchak, M. (2021, August 9). *Global climate Change: What you need to know*. National Resources Defense Council. https://www.nrdc.org/stories/global-climate-change-what-you-need-know#:~:text=Natural%20 causes%20of%20climate%20change, naturally%20 occurring%20 greenhouse%20gas%20concentrations.

Earth Observatory. (2020). *World of change: Global temperatures*. NASA. https://earthobservatory.nasa.gov/world-of-change/global-temperatures.

Energy Information Administration (EIA). (2021, July 15). *U.S. energy Information administration - eia - independent statistics and analysis*. Greenhouse gases - U.S. Energy Information Administration (EIA). https://www.eia.gov/energyexplained/energy-and-the-environment/greenhouse-gases.php.

Environmental Protection Agency (EPA). (2000, August). *Radiation Protection at EPA*. US EPA. https://www.epa.gov/sites/default/files/2015-05/documents/402-b-00-001.pdf.

Environmental Protection Agency (EPA). (2021, April 28). *CAP-88 PC*. EPA. https://www.epa.gov/radiation/cap-88-pc.

Environmental Protection Agency (EPA). (2021, February 25). *CAP-88 PC Version 4.1 Downloads and Supporting Documents*. EPA. https://www.epa.gov/radiation/cap-88-pc-version-41-downloads-and-supporting-documents.

Gupta, S. and Gupta, K. (2020). Bioaccumulation of Pesticides and Its Impact on Biological Systems. In Pesticides in Crop Production (eds P.K. Srivastava, V.P. Singh, A. Singh, D.K. Tripathi, S. Singh, S.M. Prasad and D.K. Chauhan). https://doi.org/10.1002/9781119432241.ch4.

Intergovernmental Panel on Climate Change (IPCC). (2014). *Future Changes, risks and impacts*. IPCC 5th Assessment Synthesis Report. https://ar5-syr.ipcc.ch/topic_futurechanges.php.

Met Office Hadley Center. (2018). *UKCP18 Guidance: Representative Concentration Pathways*. Met Office. https://www.metoffice.gov.uk/binaries/content/assets/metofficegovuk/pdf/research/ukcp/ukcp18-guidance---representative-concentration-pathways.pdf.

NASA. (2021, June 16). *The causes of climate change*. NASA. https://climate.nasa.gov/causes/.

National Climate Change Adaptation Research Facility (NCCARF). (n.d.). *What are the RCPs?* CoastalAdapt. https://coastadapt.com.au/sites/default/files/infographics/15-117-NCCARFINFOGRAPHICS-01-UPLOADED-WEB%2827Feb%29.pdf.

National Oceanic and Atmospheric Administration (NOAA). (2021, August 6). *How reliable are weather forecasts?* NOAA SciJinks – All About Weather. https://scijinks.gov/forecast-reliability/#:~:text=The%20Short%20Answer%3A,90%20percent%20of%20the%20time.&text=Meteorologists%20use%20computer%20programs%20called%20weather%20models%20to%20make%20forecasts.

Zobel, Z., Wang, J., Wuebbles, D. J., & Kotamarthi, V. R. (2017, December 18). *High-*

Resolution Dynamical Downscaling Ensemble projections of future extreme Temperature distributions for the United States. AGU Journals. https://agupubs.onlinelibrary.wiley.com/doi/full/10.1002/2017EF000642.

Zobel, Z., Wang, J., Wuebbles, D., & Kotamarthi, V. R. (2018, February). *Evaluations of high-resolution dynamically downscaled ensembles over the contiguous United States*. https://www.researchgate.net/publication/315899254_Evaluations_of_high-resolution_dynamically_downscaled_ensembles_over_the_contiguous_United_States.